energies

MDPI

Article

Multi-Phase Tectonic Movements and Their Controls on Coalbed Methane: A Case Study of No. 9 Coal Seam from Eastern Yunnan, SW China

Ming Li [1,2], Bo Jiang [1,2,*], Qi Miao [2,3], Geoff Wang [4], Zhenjiang You [4] and Fengjuan Lan [1,2]

1 Key Laboratory of Coalbed Methane Resources and Reservoir Formation Process, Ministry of Education (China University of Mining and Technology), Xuzhou 221116, China; cumtmingli@cumt.edu.cn (M.L.); lanfj1986@cumt.edu.cn (F.L.)
2 School of Resources and Earth Science, China University of Mining and Technology, Xuzhou 221116, China; miaoqi198@cumt.edu.cn
3 No. 198 Coalfield Geology Prospecting Team of Yunnan Province, Kunming 650208, China
4 School of Chemical Engineering, The University of Queensland, Brisbane, QLD 4072, Australia; gxwang@uq.edu.au (G.W.); z.you@uq.edu.au (Z.Y.)
* Correspondence: jiangbo@cumt.edu.cn; Tel.: +86-139-5135-9055

Received: 22 October 2020; Accepted: 16 November 2020; Published: 17 November 2020

Abstract: Multi-phase tectonic movements and complex geological structures limit the exploration and hotspot prediction of coalbed methane (CBM) in structurally complex areas. This scientific problem is still not fully understood, particularly in the Bumu region, Southwest China. The present paper analyses the occurrence characteristics and distribution of CBM based on the comprehensive analysis of CBM data. In combination with the analysis of the regional tectonics setting, geological structure features and tectonic evolution. The control action of multi-phase tectonic movements on CBM occurrence are further discussed. Results show that the Indosinian local deformation, Yanshanian intense deformation, and Himalayan secondary derived deformation formed the current tectonic framework of Enhong synclinorium. The intense tectonic compression and dextral shear action in the Yanshanian and Himalayan movements caused the complex geological structures in Bumu region, composed of the Enhong syncline, associated reverse faults and late derived normal fault. The CBM distribution is complex, which has the central and western NNE-trending high gas content zones along the syncline hinge zone and the reverse faults. The geological structure controls on CBM enrichment are definite and important. Based on geological structure features and responses of gas content, methane concentration, and gas content gradient, the gas controlling patterns of geological structure are determined and can be classified into five types: the reverse fault sealing, syncline sealing, monoclinal enrichment, normal fault dispersion, and buried floor fault dispersion types. The structural compression above the neutral surface plays an important role in the syncline sealing process, which is indicated by an increase in gas content gradient. The EW-trending tectonic intense compression and dextral shear action in the Himalayan movement avoided the negative inversion of NNE-trending Yanshanian compressive structure and its destruction of CBM reservoir. However, the chronic uplift and derived normal fault during Himalayan period caused the constant dissipation of CBM.

Keywords: coalbed methane; geological structure; gas controlling pattern; neutral surface; tectonic movement; Bumu region

1. Introduction

Coalbed methane (CBM) resources are abundant in China, where early-stage large-scale CBM development is undertaken actively [1]. However, the complex geological settings of CBM need further investigation in order to achieve large-scale commercial production efficiently [1,2]. The coal-bearing basins in China experienced multi-phase tectonic movements in geologic history and developed complex geological structures [3]. Geological structure plays an important role in the process of CBM generation, occurrence, migration, and enrichment in coal seams [4–11]. Especially, the influence on CBM occurrence from the geological structure modification of the coal reservoir physical properties, such as porosity, adsorption, and permeability [12–20]. Research has been focused on the variation of gas content with geological structure; generally, fold and fault. CBM resources within depth less than 2000 m in China are estimated to be 36.81 trillion m^3, of which more than 84% occur in nine large-scale basins, such as the Junggar, Tianshan, Tuha, Santanghu, Ordos, Qinshui, Erenhot, Hailar, and western Guizhou–eastern Yunnan basins [1]. Most of these basins exhibit the syncline or synclinorium structure. Syncline structure is a favorable area in terms of CBM reservoir formation, mainly due to the increase in coal seam buried depth and gas content [7,21]. On the other hand, the compression above the neutral surface and the extension below the neutral surface of the syncline are also important for the CBM occurrence [22–24]. However, there is still a lack of effective methods for determining the neutral surface and its effects on CBM. The influence of fault structure on CBM is generally summarized as gas contents are usually higher near the reverse faults and lower adjacent to the normal faults [1,25]. The normal faults can also increase the gas content in closed and occluded types [9]. The early faults are mainly modified and reversed during the late tectonic movement, especially the early compression and late extension. The evolution of fault and the effects of geological structure on other gas-bearing characteristics, such as the gas composition, gas pressure, and gas content gradient, are still not well understood.

The Enhong synclinorium is located in the eastern Yunnan region, Southwest China, with abundant coal resources (Figure 1) [26]. The coal-bearing stratum is the Upper Permian Changxing Formation (P_3c) and Longtan Formation (P_3l). The estimated coal-bearing area is about 485 km^2. The geological coal reserves with burial depth less than 2000 m is 5.25×10^9 tons, which makes this synclinorium one of the largest coking coal producing areas in China [27]. The amount of CBM resources with burial depth less than 2000 m is 6.13×10^{10} m^3, and 82% of the volume is located at a depth less than 1000 m, showing a good prospect for CBM exploitation [28]. 12 CBM wells have been drilled in the research area. However, the Enhong synclinorium is characterized by the complex geological structure, which is composed of various scales and orientations of dense folds and faults. The complex structure restricts the exploration and commercial exploitation of CBM. Considering the complexity of the geological structure, as well as the insufficient and uneven CBM data for the whole region, this work takes the Bumu region as the research area because of the rich geological and CBM data available, which is located in the central part of the Enhong synclinorium.

This article presents the occurrence characteristics and distribution of CBM based on the comprehensive analysis of those CBM data. Multi-phase tectonic movements in structurally complex CBM fields are determined according to the analysis of the regional tectonics setting, geological structure features and structural evolution. The gas controlling patterns of geological structure are jointly proposed by the multiple CBM parameters analysis. The multi-phase tectonic movements controls on CBM occurrence are further discussed. The results of this study provide new insights and improved understanding of the influence of fold neutral surface and fault sealing on CBM, which may have significant implications for CBM exploitation in structurally complex areas.

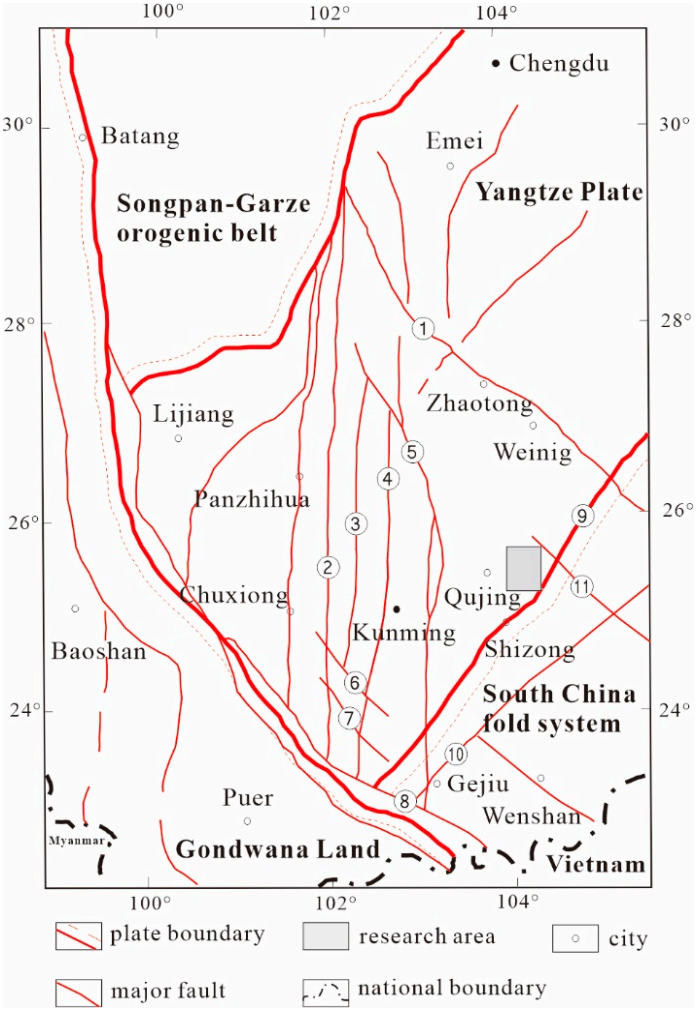

Figure 1. Tectonic location of the study area.1-Weining-Ziyun-Nandan fault, 2-Anninghe-Lvzhijiang fault, 3-Luoci-Yimen fault, 4-Puduhe-Dianchi fault, 5-Xiaojiang fault, 6-E'shan-Tonghai fault, 7-Huanian fault, 8-Red river fault, 9-Mi'le-Shizong fault, 10-Nanpanjiang fault, 11-Youjiang fault.

2. Geological Setting

2.1. Regional Structure

The research area is tectonically located in the southwestern margin of the Yangtze plate (Figure 1). It occurs at the boundary between the Tethys-Himalaya tectonic domain and the circum Pacific tectonic domain [29,30]. This tectonic unit is bordered by the NE-trending Mi'le-Shizong fault in the south, the NS-trending Xiaojiang fault in the west and the NW-trending Youjiang fault in the northeast [31,32].

The Bumu region is located in the central part of the Enhong synclinorium, which is the main geological structure in this area (Figure 2). The Enhong synclinorium, with a length of 53 km and width of 6–12 km, is located between the NE-trending Fuyuan-Mi'le fault and the NS-trending Pingguan-Agang fault [33]. The Enhong synclinorium is mainly composed of Enhong syncline and many secondary anticlines and synclines, which extend in the direction of NE, NNE, NS, and NNW from the southwest to the northeast of the Enhong synclinorium. The deformation strength of the fold decreases gradually from west to east and from north to south, with the stratigraphic dip angle of about 10–25°. Meanwhile, the NE-plunging Enhong synclinorium is strongly destroyed by numerous multilevel multidirectional faults (Figure 2). The secondary derived drag folds, derived faults, and associated faults developed well in the northwestern limb of Enhong synclinorium. The derived brachy drag folds in the south are mainly arranged in echelons to the right row, and the axial traces

form an acute angle with the Fuyuan-Mi'le fault, indicating that the deformation mechanism of the folds is derived from the right-lateral slipping of the Fuyuan-Mi'le fault (Figure 2). The NE-trending secondary associated folds are strongly deformed and extend near the fault zone of Fuyuan-Mi'le fault. The secondary faults in the northwestern limb are mostly the NNE-trending derived faults and the NE-trending associated branch faults of the Fuyuan-Mi'le fault.

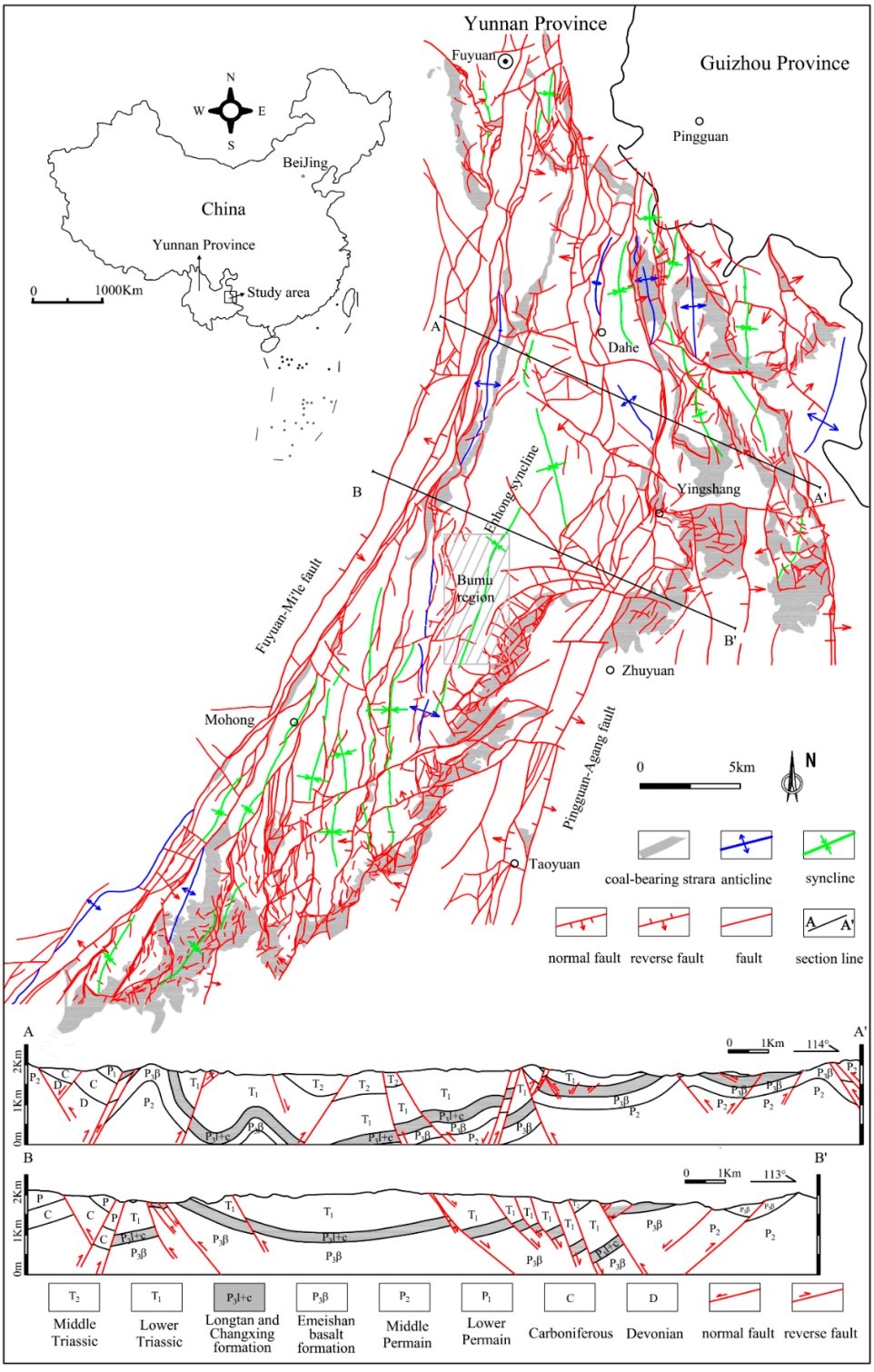

Figure 2. Geological sketch map and structural cross section of Enhong synclinorium.

The NS- and NNW-trending folds developed well in the north part of the southeastern limb of the Enhong synclinorium (Figure 2). The secondary faults in the southeastern limb are commonly the NS-trending associated faults and the NE-, EW-, and NW-trending strike-slip normal derived faults, which are mostly arranged as an echelon pattern and are restricted by the Pingguan-Agang fault at a large angle. Especially the arcuate fault zone, composed by the right-lateral strike-slip normal faults, is formed near the eastern part of the Bumu region. Additionally, the latter small oblique strike-slip faults, mainly the NNW-trending left-lateral strike-slip faults and NEE-trending right-lateral strike-slip faults, cut across the major structure and complicate geological structure.

2.2. Coal-Bearing Strata and Coal Seam

The basement of the Yangtze plate in this area is the Mesoproterozoic Kunyang Group. The sedimentary stratum are Siluric, Devonian, Carboniferous, Permian, Triassic, Paleogene, Neogene, and Quaternary [29]. The exposure strata in the research area are mainly the limestone of Yongningzhen Formation (T_1y) and the siltstone and sandstone of Feixianguan Formation (T_1f). The buried strata, exposed by drilling, are Kayitou Formation (T_1k), Changxing Formation (P_3c), Longtan Formation (P_3l) and Emeishan basalt Formation ($P_3\beta$) (Figure 3a). The Changxing Formation (P_3c) and Longtan Formation (P_3l) are the major coal-bearing strata. They were measured between 214.33 m to 278.55 m in thickness and consist of 28 to 46 coal seams (Figure 3a). The total thickness of the coal seams ranges from 20.23 m to 35.54 m with an average thickness of 30.22 m. The minable coal seams are the coal seams Nos. 4, 7–9, 12, 13, 15, 16, and 18–24, with an average thickness of 19.57 m, and the $R_{o,max}$ ranges from 1.07% to 1.15% (Table 1). The thickness, coal quality, and lateral stability of coal seams in the upper segment of Longtan Formation (P_3l^2) are favorable for the exploitation of coal and CBM. The No. 9 coal seam, with a thickness of 1.22–5.80 m and an average thickness of 3.28 m, is stable and the unique regional minable coal seam in the research area.

Table 1. Characteristic and gas content of main coal seam in the Bumu region.

Stratum	Coal Seam	Thickness (m)	$R_{o,max}$ (%)	Coal Maceral (%)			V_{daf} (%)	Gas Composition (%)			Gas Content (m^3/t)
				V	*I*	*L*		CH_4	C_{2+}	N_2	
P_3c	4	1.06	1.08	67.9	9.4	22.7	30.92	63.33	5.31	30.07	9.25
P_3l^2	7	1.18	–	71.0	6.7	22.3	28.85	66.70	9.60	22.07	11.06
P_3l^2	8	0.90	1.09	69.0	5.0	26.0	28.40	–	–	–	–
P_3l^2	9	3.28	1.10	64.9	10.9	24.2	29.74	66.93	9.54	22.72	11.21
P_3l^2	12	1.75	1.08	66.4	9.8	23.8	27.71	59.91	13.48	24.65	9.15
P_3l^2	13	0.73	–	66.3	9.6	24.1	25.78	71.33	7.46	20.19	13.17
P_3l^2	15	1.64	1.07	66.2	8.7	25.1	27.37	65.86	11.73	20.95	14.00
P_3l^1	16	1.43	1.08	66.6	9.5	23.9	26.89	67.92	10.98	19.17	10.64
P_3l^1	18	0.87	1.09	66.6	11.1	22.3	26.96	65.74	10.83	21.48	13.52
P_3l^1	19	0.98	1.08	64.8	14.2	21.0	25.35	–	–	–	–
P_3l^1	20	0.83	1.07	68.2	10.1	21.7	25.53	71.32	12.37	15.03	12.34
P_3l^1	21	1.40	1.11	63.1	11.2	25.7	26.41	73.93	11.12	13.50	12.31
P_3l^1	22	1.32	–	68.1	7.9	24.0	26.19	71.85	14.75	12.45	12.58
P_3l^1	23	1.26	1.15	62.6	12.7	24.7	26.41	46.57	3.63	48.52	7.94
P_3l^1	24	1.11	1.09	67.2	12.5	20.3	26.50	–	–	–	–

Note: $R_{o,max}$—maximum vitrinite reflectance, V_{daf}—volatile yield (dry ash-free base), *V*—vitrinite, *I*—inertinite, *L*—liptinite.

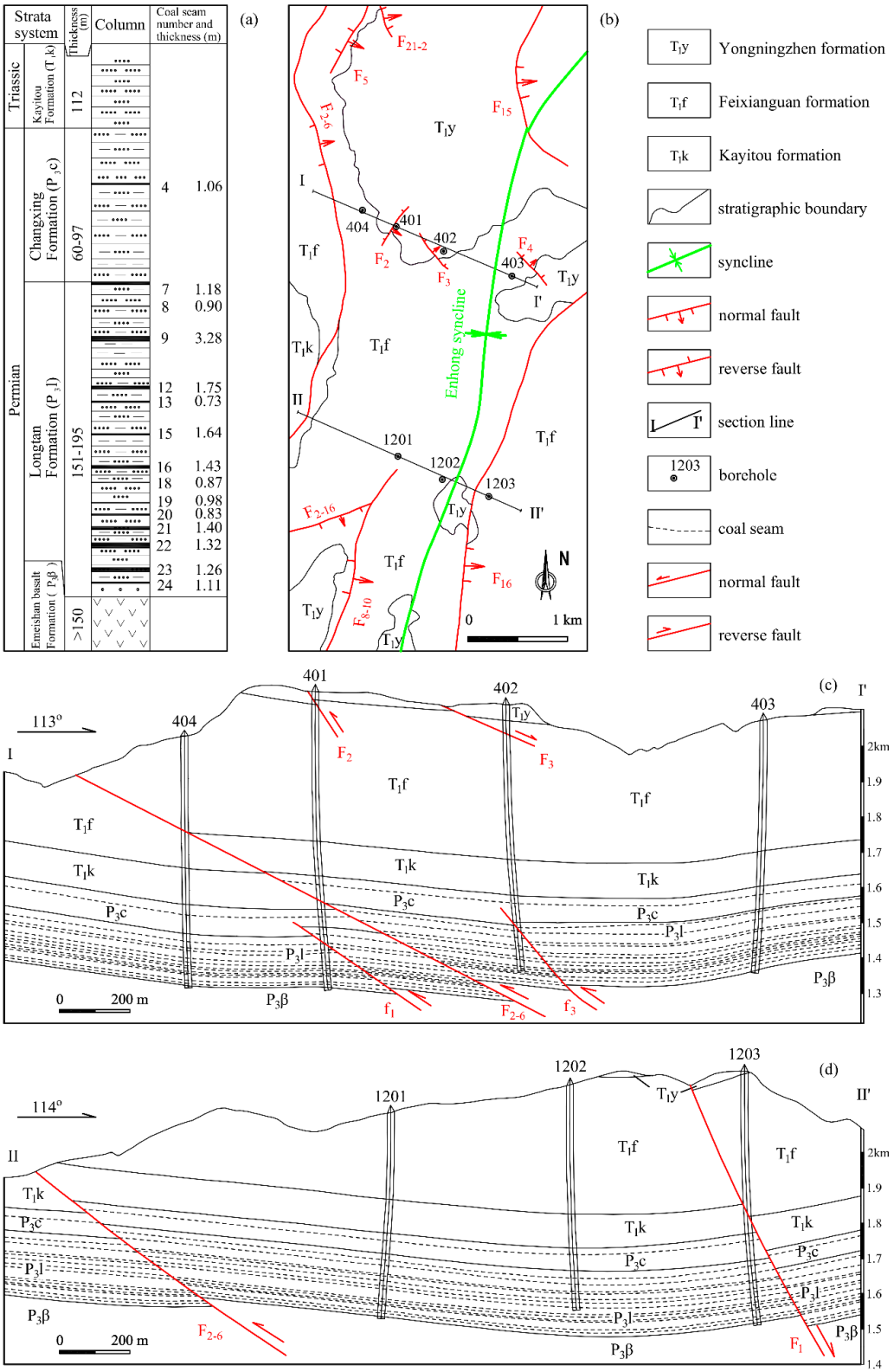

Figure 3. Stratigraphic column of coal-bearing strata (**a**), structural outline map (**b**) and structural cross sections (**c**,**d**) of Bumu region.

3. Material and Experimental Methodology

The geological structures and structural features in Bumu region were analyzed and determined according to the field and drilling geological surveys. The structural features, distribution law, structural

pattern, and mechanical causes of numerous multilevel folds and faults of Enhong synclinorium in the region were systematically studied based on the theory of modern structural geology and geomechanical analysis. In combination with the analysis of regional tectonic setting, the multi-phase tectonic evolution and deformation mechanism in the research area were discussed and determined.

The CBM gas content and gas components of 108 coal samples from different coal seams in Bumu region were measured according to the desorption method and gas chromatography method that following Chinese National Standards GB/T 19559-2008 and GB/T 13610-2003, respectively (Table 1). The No. 9 coal seam has the most CBM data, obtained from 27 boreholes (Table 2). The maximum vitrinite reflectance measurement, coal maceral composition analysis, and proximate analysis were performed following the Chinese National Standards GB/T6948-2008, GB/T8899-1998, and GB/T212-2008, respectively (Table 1). These CBM data form the basis for the discussion of the occurrence characteristics and distribution of CBM in Bumu region. Based on the response and variation of CBM gas content, gas component and gas content gradient to the different types and periods geological structures, the control action of different geological structures, fold neutral surface action and fault sealing in multi-phase tectonic movements on CBM occurrence were further discussed.

Table 2. List of gas-bearing property parameters and structure position of No. 9 coal seam.

Borehole	Depth (m)	Gas Content (m^3/t)	CH_4 Concentration (%)	Gas Content Gradient (m^3/t/100 m)	Structure Position	Gas Controlling Pattern *
0103	472.92	15.30	75.37	3.24	Hanging wall of $F_{8–10}$	I
103	503.85	13.41	72.54	2.66	Hanging wall of $F_{8–10}$	I
301	531.76	19.27	83.40	3.62	Footwall of $F_{2–6}$	I
301-1	402.67	15.30	73.90	3.80	Hanging wall of $F_{2–6}$	I
404	587.74	13.61	91.09	2.32	Footwall of $F_{2–6}$	I
0101	489.24	9.72	71.66	1.99	Hinge zone of syncline	II
101	578.86	10.50	67.03	1.81	Hinge zone of syncline	II
1202	564.99	15.03	78.98	2.66	Hinge zone of syncline	II
403	564.77	10.97	67.95	1.94	Hinge zone of syncline	II
504	688.21	14.65	92.02	2.13	Hinge zone of syncline	II
505	683.71	9.11	90.86	1.33	Hinge zone of syncline	II
602	838.12	10.93	92.02	1.30	Hinge zone of syncline	II
501	687.98	7.31	61.62	1.06	NWW limb of syncline	III
502	767.14	9.10	53.76	1.19	NWW limb of syncline	III
503	731.10	11.71	51.58	1.60	NWW limb of syncline	III
1201	435.25	11.20	71.97	2.57	NWW limb of syncline	III
2301	490.30	10.25	66.81	2.09	NWW limb of syncline	III
EH01	265.07	7.79	89.85	2.94	SEE limb of syncline	III
0102	468.32	8.39	70.19	1.79	Footwall of F_{16}	IV
102	509.22	9.59	75.82	1.88	Footwall of F_{16}	IV
1203	574.00	10.31	49.67	1.80	Footwall of F_{16}	IV
2302	566.00	9.81	57.13	1.73	Footwall of F_{16}	IV
303	554.54	9.38	57.55	1.69	Footwall of F_{16}	IV
401	688.09	11.50	63.74	1.67	Hanging wall of f_1	V
402	646.40	9.70	42.16	1.50	Footwall of f_3	V
4501	715.42	9.91	31.72	1.39	Hanging wall of F_2	V
4503	623.72	11.1	45.65	1.78	Footwall of f_4	V

* Gas controlling pattern: I—reverse fault sealing type, II—syncline sealing type, III—monoclinal enrichment type, IV—normal fault dispersion type, V—buried floor fault dispersion type.

4. Geological Structure and Tectonic Evolution

The geological structures in Bumu region are mainly the Enhong syncline, reverse, and normal faults (Figure 3b). The Enhong syncline is the main geological structure, which controls the overall distribution, orientation, and burial depth of coal seams (Figure 3c,d). The Enhong syncline is an open NNE-plunging symmetrical syncline, with the hinge line plunges in the direction of NE17° and the plunge angle of 15–30°. The coal seams are generally distributed in NE and NW direction, with a dip angle of about 5–20° in the south and about 15–30° in the north.

Geological survey has discovered 20 faults, developed well in this area with the directions of NNE, NE, and NW (Figure 3b). The faults are mainly reverse faults, with a few normal faults. The reverse faults are mostly in NNE direction and the normal faults are mostly in NE and NW directions. The imbricate large reverse faults of $F_{2–5}$, $F_{2–6}$, $F_{8–10}$, and F_5, with the fault throw of 40–55 m, are located in the NWW limb of Enhong syncline (Figure 3c). The normal faults are limited by the NNE-trending reverse faults and that indicates the normal faults are formed later. Normal faults generally extend unsteadily, especially the F_{16} fault, as the southern section of the arcuate strike-slip normal derived faults, extends in NE–NEE direction. There are seven faults, $F_{2–6}$, $F_{8–10}$, F_{16}, f_1, f_2, f_3, and f_4 in No. 9 coal seam.

Since the formation of coal measures in the Late Permian, the study area has mainly experienced Indosinian movement, Yanshanian movement, and Himalayan movement. Affected by the NW-trending basement fault on the northeast, the NW-trending folds and reverse faults were formed beside the basement faults under the NS-trending tectonic compression in the Indosinian [34]. In other areas of the Enhong synclinorium, including the Bumu region, the influence of the Indosinian movement was very weak and the Indosinian geological structure was rare. During the late Jurassic and early Cretaceous, the subduction of the Pacific plate and the compression of the South China block led to the intense Yanshanian tectonic movement [35]. The intense tectonic compression in the direction of NW–SE caused formation of the Enhong syncline, Fuyuan-Mi'le fault, Pingguan-Agang fault, and the associated branch faults. In the Bumu region, the NNE-trending large reverse fault of $F_{2–6}$ and $F_{8–10}$, as well as small buried reverse fault of f_1, f_2, f_3, and f_4 were formed (Figure 3). The former Indosinian NW-trending structures ware modified intensely and the Yanshanian NE-trending structures were formed rarely in the northeast of the Enhong synclinorium. During the Eocene, the northward subduction of the Indian plate and the westward subduction of the Pacific plate for the Eurasian plate caused the Himalayan movement, EW-trending tectonic compression and dextral shear action [36–38]. It caused a right-lateral shear slip and property transformation of the Fuyuan-Mi'le fault and the Pingguan-Agang fault. Meanwhile, the formation of the NNE-trending secondary derived drag folds and derived compression-shear faults in the NW limb, combined with the NE- and EW-trending strike-slip normal derived faults in the SE limb complicated and formed the current tectonic framework of the Enhong synclinorium. The derived normal fault of F_{16} were formed in the southeast of the Bumu region. The Indosinian NW-trending structures in the northeast, the Yanshanian NNE-trending Enhong syncline, large boundary, and associated branch reverse faults, combined with the Himalayan secondary derived faults and drag folds, formed the current tectonic framework of the Enhong synclinorium.

5. Gas Occurrence Features

5.1. Gas Composition

In the Bumu region, the composition of CBM is complex, mainly composed of CH_4, N_2, CO_2, and heavy hydrocarbon gases. The heavy hydrocarbon gases (C_{2+}) include ethane and propane in the research area. The concentration of CH_4 varies greatly and ranges from 9.17% to 95.32%, with an average value of 65.60%. The N_2 and CO_2 account for 21.76% and 1.61%, respectively. The concentration of heavy hydrocarbon gas is abnormally high, 0.30–25.51%, and the average value is up to 10.47%. The CBM $\delta^{13}C_1$ ranges from −51.69‰ to −43.43‰ with an average of −46.57‰, indicating that CBM is mainly the pyrolysis product of humic organic matter and possibly the secondary biogenic gas in the shallow coal seam [39]. The local high concentration of heavy hydrocarbon gas is mainly the complete result of the coal maceral, microbial degradation, and coal pore structure [29,33].

There is no apparent linear relationship between the CBM composition and coal burial depth, indicating that the geological influence factors of CBM are complex. The concentrations of methane, heavy hydrocarbon and alkane gas generally tend to increase with coal burial depth (Figure 4a–c), while the N_2 concentration decreases with the increase in coal burial depth (Figure 4d).

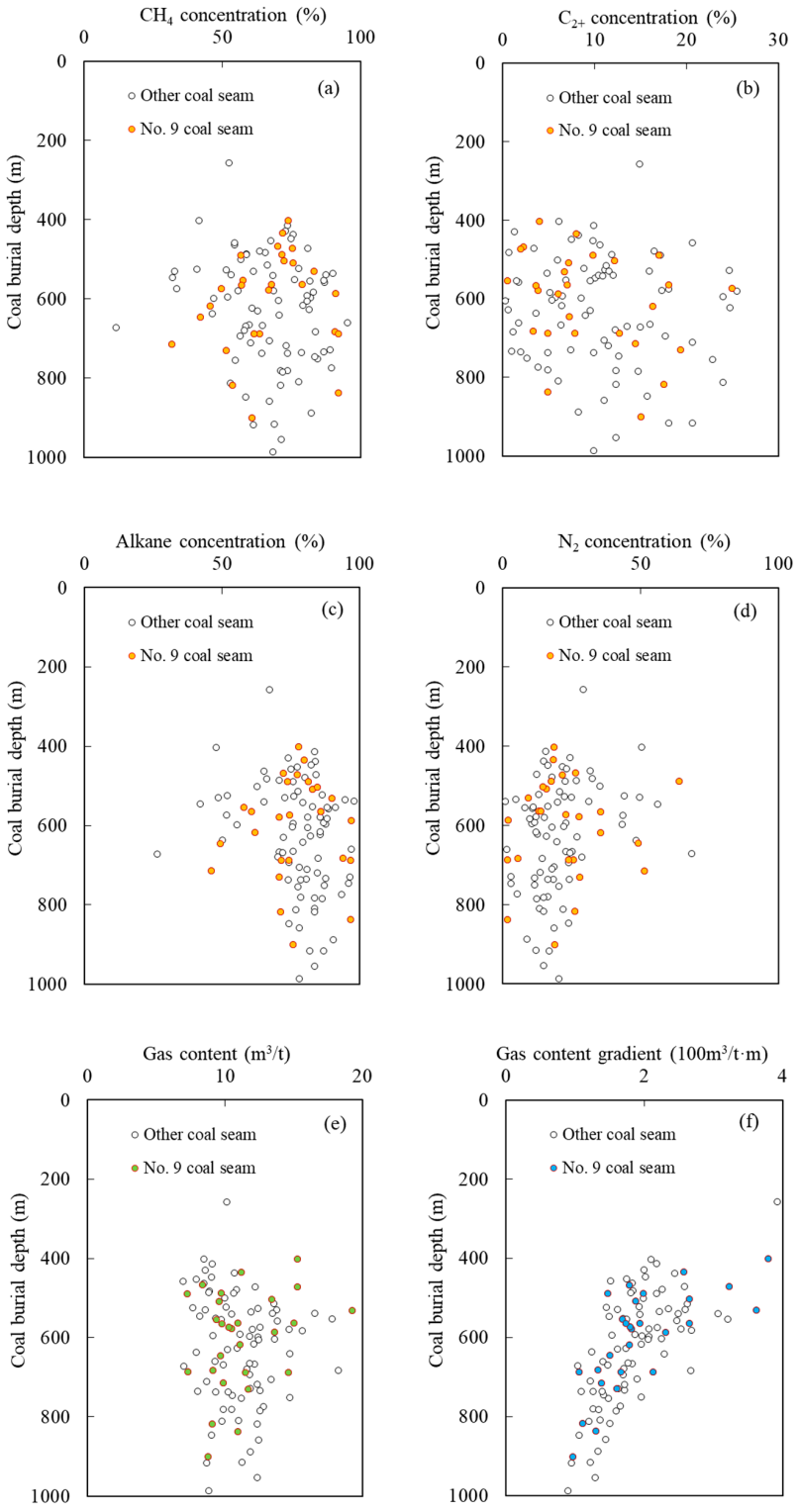

Figure 4. The gas-bearing property parameters vary with the coal burial depth. (**a**) methane concentration, (**b**) heavy hydrocarbon gas concentration, (**c**) alkane concentration, (**d**) N_2 concentration, (**e**) gas content, and (**f**) gas content gradient.

In the Bumu region, the methane concentration of CBM decrease while as the N_2 and heavy hydrocarbon gas concentration increase. The dissipation of methane, as well as its mutual exchange and mixture with surface atmosphere are mostly the main geological cause. It indicates that the CBM

occurrence space in the study area has relatively low sealing capacity, which may have resulted from destruction of fault in the CBM reservoir. This is consistent with the complicated geological structure in the Bumu region.

5.2. Gas Content and Its Distribution

In the Bumu region, the gas content of coal seam ranges from 6.94 to 19.27 m^3/t and is mainly between 8 and 13 m^3/t. The average value of gas content is 11.19 m^3/t. Generally, the CBM content tends to increase linearly with coal burial depth and the gas content gradient tends to decrease with coal burial depth following the power function [40]. With the increase in the coal burial depth, the gas content gradient exhibits an overall decreasing trend, but there is no significant positive correlation with the gas content in the Bumu region (Figure 4e,f). The overall relatively low methane concentrations and gas contents of coal seam indicate the widely distributed open and semi-open reservoir space of CBM in the study area. The influence of geological structure on the sealing of CBM reservoir is important and will be discussed in greater detail later in this paper. The gas content of different coal seams fluctuate significantly with stratigraphic sequence and these observations were previously interpreted as a result of multiple unattached CBM-bearing systems in the vertical section [41,42]. Therefore, this study selects the No. 9 main coal seam with stable development and largely available gas data as the research object to discuss the gas distribution features (Table 2, Figure 5).

Gas content of No. 9 coal seam in the Bumu region is relatively high, ranging from 7.31 to 19.27 m^3/t and with an average value of 11.29 m^3/t. The distribution pattern of gas content is complex and has an overall banding distribution in the direction of NNE. The CBM enrichment region, with the gas content higher than 10 m^3/t and about half of the study area, is distributed along the hinge zone of the Enhong syncline. The gas contents of the two limbs of syncline decrease and form two low gas content zones in the northwest and southeast of the study area. At the same time, the development of fault structures complicates the geological structure and the occurrence of CBM in the study area, resulting in the further differentiation of CBM content distribution, particularly in the west (Figure 5). With the gas content of 10 m^3/t as the boundary, the central NNE-trending high gas content zone, western NNE-trending high gas content zone, northwest, and southeast low gas content zones can be further divided as follows.

(1) Central NNE-trending high gas content zone, with a length of 6500 m in the NNE direction and a width about 1500 m. The gas content is 10.25–15.30 m^3/t, with an average of 12.11 m^3/t. Meanwhile, two secondary high gas content zones have been formed in the southwest and northeast, with the gas content generally higher than 13 m^3/t and 11 m^3/t, respectively. The distribution of gas content gradient is similar to that of gas content, and there is an overall trend that the gas content gradient decreases from the southwest to the northeast, in the direction of the Enhong syncline plunging. However, the methane concentration of CBM is high in the southwest and northeast while is low in the central region.

(2) In the western NNE-trending high gas content zone, the gas content, gas content gradient, and methane concentration vary greatly and distribute complexly. The gas content is 9.70–19.27 m^3/t and the highest gas content zone forms in the study area. The gas content gradient is 1.50–3.62 m^3/t/100 m and the methane concentration is 42.16–83.40%.

(3) In the northwest low gas content zone, the gas content, gas content gradient, and methane concentration are all low, with the mean value of 8.77 m^3/t, 1.21 m^3/t/100 m and 49.03%, respectively. Such a situation is very unfavourable for the CBM accumulation.

(4) In the southeast low gas content zone, the gas content is 7.79–9.81 m^3/t, with its contour lines extending in NNE direction and decreasing in SEE direction. In general, the contour lines of gas content gradient and methane concentration also extend in NNE direction, while decreasing in NWW direction.

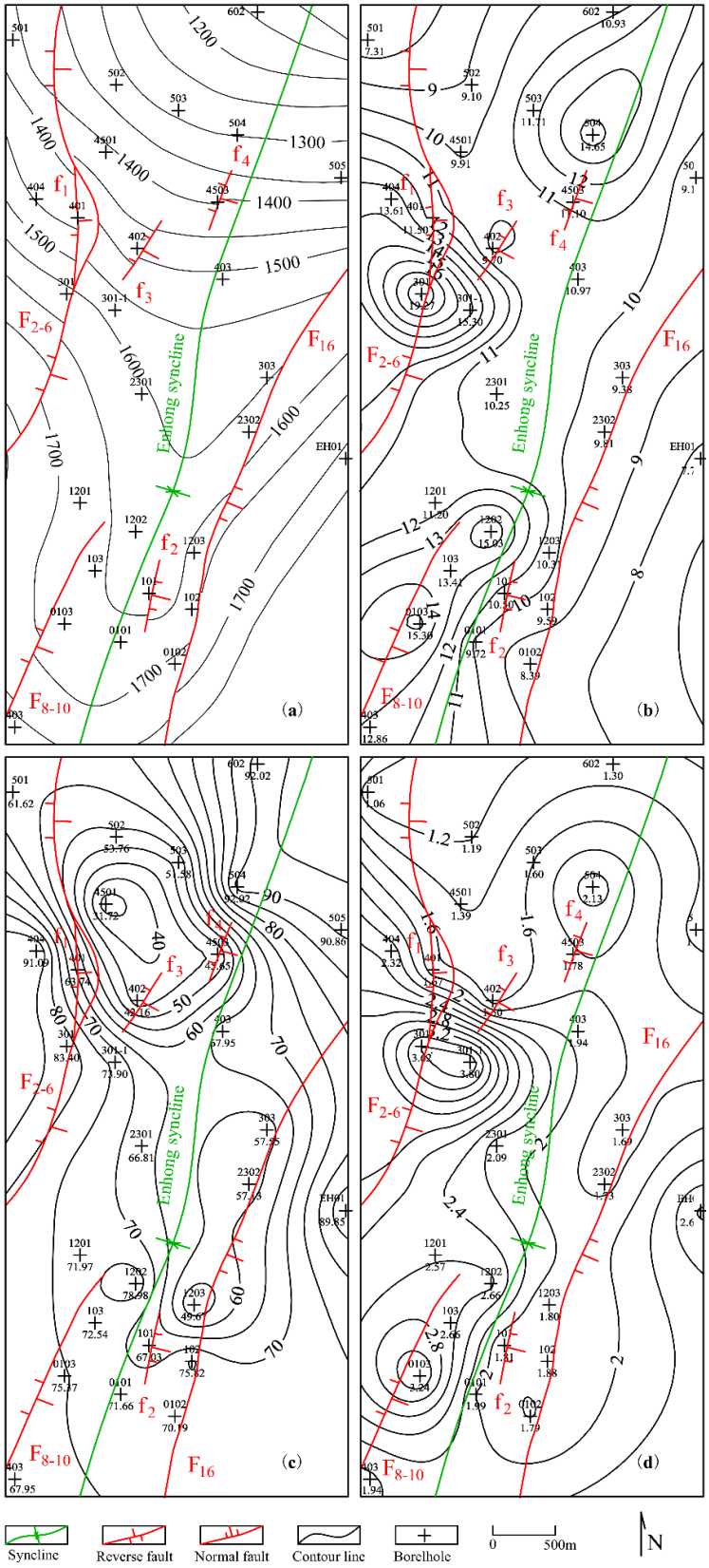

Figure 5. Contour maps of No. 9 coal seam floor, structural sketch and gas-bearing property parameters. (**a**) coal seam floor and structural sketch; (**b**) gas content; (**c**) methane concentration; (**d**) gas content gradient.

6. Gas Controlling Pattern of Geological Structure

In the Bumu region, as a complex geologic structural area with well-developed syncline, normal fault and reverse fault structures, geologic structures play an important role in the occurrence and distribution of CBM, especially the effects of multi-phase tectonic movements after the formation of coal seam. A systematic study on the structural characteristics, tectonic evolution, and CBM occurrence shows that the gas distribution pattern is mainly controlled by the development of geological structures. The development of the Enhong syncline leads to the deep burial and structural compression of the coal seam in the syncline hinge zone, which could allow gas enrichment and shows that the central NNE-trending high gas content zone spreads along the Enhong syncline axis and an overall decreasing trend from the hinge zone of the Enhong syncline, in the central NNE-trending high gas content zone, to its limbs in the northwest and southeast low gas content zones. The development of different types of fault structures further complicates the geological structure and CBM content distribution in the study area, especially in the western NNE-trending high gas content zone.

According to the variation of gas content, gas content gradient, and methane concentration in different structure parts, the effects of different geological structures on CBM occurrence are determined as the following five types: reverse fault sealing type, syncline sealing type, monoclinal enrichment type, normal fault dispersion type, and buried floor fault dispersion type (Figure 6).

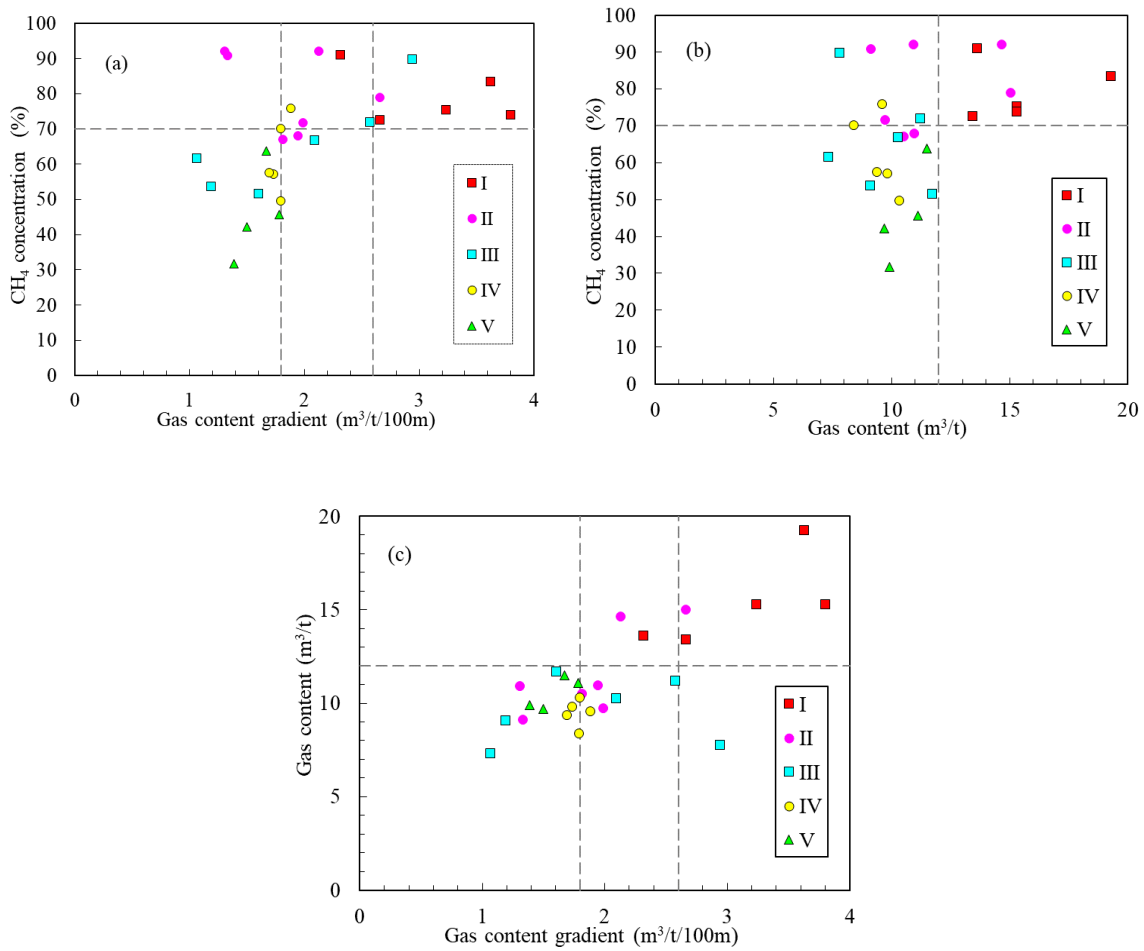

Figure 6. Scatter diagram of gas-bearing property parameters of 5 gas controlling pattern. (**a**) plot of methane concentration to gas content gradient; (**b**) plot of methane concentration to gas content; (**c**) plot of gas content to gas content gradient. Gas controlling pattern: I—reverse fault sealing type, II—syncline sealing type, III—monoclinal enrichment type, IV—normal fault dispersion type, V—buried floor fault dispersion type.

(1) Reverse fault sealing type: No. 9 coal seam from boreholes Nos. 0103, 103, 301, 301-1, and 404 is characterized by the high value of gas content, methane concentration, and gas content gradient, which is generally higher than 12 m^3/t, 70% and 2.6 m^3/t/100 m, respectively. The mean values of those properties in the test boreholes are 15.38 m^3/t, 79.26% and 3.13 m^3/t/100 m, respectively. Those boreholes are located near the large reverse fault of $F_{2–6}$ and $F_{8–10}$, which are formed during the Yanshanian period. Compared with the Yanshanian reverse faults in the North China plate that are mostly reversed to the normal faults in the later period [7], the Yanshanian large reverse fault, even underwent the strike-slip structural modification during the Himalayan period, still have good seal capacity and are beneficial for the preservation of CBM.

(2) Synclinal sealing type: No. 9 coal seam is characterized by the high gas content, methane concentration and the medium gas content gradient, which is generally higher than 10 m^3/t, 70%, and about 2.0 m^3/t/100 m, respectively (Table 2). The CBM of No. 9 coal seam from boreholes Nos. 0101, 101, 1202, 403, 504, 505, and 602, located in the hinge zone of the Enhong syncline, has a mean value of 11.56 m^3/t, 80.07% and 1.88 m^3/t/100 m, respectively. The development of syncline leads to the increase in coal seam burial depth, which is conducive to the accumulation of CBM and the increase in gas content from limb to hinge zone. In contrast, the gas content gradient tends to decrease with the increase in the burial depth [40]. Therefore, the increase in the gas content gradient of coal seam in the Enhong syncline hinge zone, compared to the limbs, is strong evidence that the structural compression above the neutral surface is conducive to the accumulation of CBM.

(3) Monoclinal enrichment type: No. 9 coal seam located in syncline limbs, such as Nos. 501, 502, 503, 1201, 2301, and EH01 boreholes, is characterized by the medium gas content, methane concentration and the low gas content gradient, which is generally lower than 12 m^3/t, 70% and about 1.8 m^3/t/100 m, respectively (Table 2). The gas content gradient varies greatly, ranges from 1.06 to 2.94 m^3/t/100 m, which is caused by its decrease with the increase in burial depth.

(4) Normal fault dispersion type: No. 9 coal seam located in the footwall of F_1 normal fault, such as Nos. 0102, 102, 1203, 2302, and 303 boreholes, is characterized by the low gas content, methane concentration, and gas content gradient, which is generally lower than 10 m^3/t, 70%, and about 1.8 m^3/t/100 m, respectively (Table 2). The right-lateral slipping of the Pingguan-Agang fault derives the F_{16} normal fault during the Himalayan period. The extensional fault destroys the CBM reservoir and provides seepage channels for CBM dissipation as well as its mutual exchange with the surface atmosphere.

(5) Buried floor fault dispersion type: No. 9 coal seam located near the buried f_1, f_3, and f_4 reverse faults is characterized by the low gas content, methane concentration, and gas content gradient, which is generally lower than 10 m^3/t, 60%, and about 1.8 m^3/t/100 m, respectively (Table 2). The scale and displacement of these buried floor faults are small, which fail to form a good sealing property for CBM. In addition, the faults penetrate the Emeishan basalt formation underlying the coal-bearing strata, and it has been reported that natural gas can be migrated and be stored in the Emeishan basalt [43,44]. The well-developed fractures in the basalt also serve as an escaping path and as a reservoir of CBM, respectively [40]. These fractures destroy the sealing of the fault and cause the dispersion of CBM.

For No. 9 coal seam in the Bumu region, methane concentration is sensitive to the sealing of CBM reservoir and is generally larger than 70% in reverse fault and syncline sealing types (Figure 6). Gas content and gas content gradient vary greatly with burial depth resulted from the different geological structure control action (Figure 7).

Gas content gradient can indicate the influence of geological structure on CBM reservoir from the buried depth, which is lower than 1.8 m^3/t/100 m in normal and buried floor fault dispersions while is higher than 2.4 m^3/t/100 m in reverse fault sealing type (Figures 6 and 7). Gas content is an important parameter for the enrichment of CBM, which is higher than 12 m^3/t in reverse fault type and around 12 m^3/t in syncline sealing type.

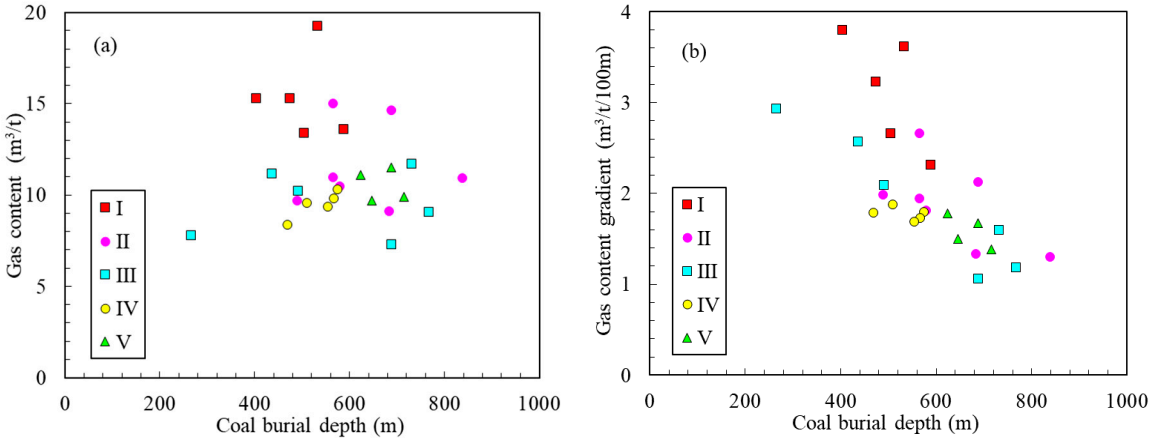

Figure 7. Gas content (**a**) and gas content gradient (**b**) vary with coal burial depth. Gas controlling pattern: I—reverse fault sealing type, II—syncline sealing type, III—monoclinal enrichment type, IV—normal fault dispersion type, V—buried floor fault dispersion type.

The tectonic movement was dominated by the continuous subsidence movements after the coal-bearing strata deposited in the Late Permian until the Late Jurassic. According to the previous numerical simulation research about the burial and thermal histories of coal seams based on the analysis of vitrinite reflectance and homogenization temperature of fluid inclusion, the largest ancient burial depth of the coal seams can reach 3800 m in the research areas [45–47]. Under the effect of paleotemperature, the coal seams experienced deep metamorphism and reached the fat coal stage, accompanied with the massive CBM generation [45,46]. The influence of the Indosinian movement was very weak and the Indosinian geological structure was rare in the Bumu region. The intense tectonic compression and the formation of compressive structures during the Yanshanian movement, as well as the peak-period of gas generation, are conducive to CBM enrichment. The gas-controlling pattern is manifested as the reverse fault sealing, syncline sealing, and monoclinal enrichment of CBM, which are the main controlling factors to the central and western NNE-trending high gas content zones. The tectonic intense compression and dextral shear action in the Himalayan movement avoided the inversion of compressive structure to extensional structure and the destruction of CBM reservoir, which are common in the North China plate [48]. However, the chronic uplift and derived normal fault during the Himalayan period caused the constant dissipation of CBM. The normal fault dispersion and buried floor fault dispersion are the main reasons for the northwest and southeast low gas content zones in the Bumu region.

7. Conclusions

Based on the largely available geological and CBM data, a comprehensive analysis is performed on the Bumu region, one of the hotspots of CBM development in Southwest China. This study has drawn several conclusions, as follows:

(1) The Indosinian local deformation, Yanshanian intense deformation, and Himalayan secondary derived deformation formed the current tectonic framework of Enhong synclinorium. The intense tectonic compression and dextral shear action in the Yanshanian and Himalayan movements caused the complex geological structures in Bumu region, which are composed of the Enhong syncline, associated reverse faults and late derived normal fault.

(2) The methane concentration of CBM decreases while the nitrogen and heavy hydrocarbon gas concentrations increase in Bumu region. The relatively low methane concentration and gas content imply the open to semi-open reservoir space of CBM. The CBM distribution is complex, which has the central and western NNE-trending high gas content zones along the syncline hinge

zone and the reverse faults. The geological structure controls on CBM enrichment are definite and important.

(3) Based on geological structure features and responses of gas content, methane concentration and gas content gradient, the gas controlling pattern of geological structure are determined and can be classified into five types: the reverse fault sealing, syncline sealing, monoclinal enrichment, normal fault dispersion, and buried floor fault dispersion types.

(4) The structural compression above the neutral surface plays an important role in the syncline sealing process, which is indicated by the increase in gas content gradient. The EW-trending tectonic intense compression and dextral shear action in the Himalayan movement avoided the negative inversion of NNE-trending Yanshanian compressive structure and its destruction of CBM reservoir. However, the chronic uplift and derived normal fault during Himalayan period caused the constant dissipation of CBM.

Author Contributions: B.J. and Q.M. conceived the ideas; M.L. analyzed the data and wrote the paper; G.W., Z.Y. and F.L. provided language and technical support. All authors have read and agreed to the published version of the manuscript.

Funding: This research was funded by National Science and Technology Major Project (2016ZX05044), National Natural Science Foundation of China (Nos. 41402136, 41702172) and Natural Science Foundation of Jiangsu Province (No. BK20140183).

Acknowledgments: The Author Ming Li thanks the China Scholarship Council (CSC) providing financial support for the collaborative research visiting in School of Chemical Engineering at the University of Queensland Australia. We would like to thank the reviewers and editors for their constructive comments and suggestions.

Conflicts of Interest: The authors declare no conflict of interest.

References

1. Qin, Y.; Moore, T.; Shen, J.; Yang, Z.B.; Shen, Y.L.; Wang, G. Resources and geology of coalbed methane in China: A review. *Int. Geol. Rev.* **2018**, *60*, 777–812. [CrossRef]
2. Tao, S.; Chen, S.D.; Pan, Z.J. Current status, challenges, and policy suggestions for coalbed methane industry development in China: A review. *Energy Sci. Eng.* **2019**, *7*, 1–16. [CrossRef]
3. Cao, D.Y.; Ning, S.Z.; Guo, A.J.; Li, H.T.; Chen, L.M.; Liu, K.; Tan, J.Q. *Tectonic Framework of Coalfields and Tectonic Control of Coal Seams in China*; Science Press: Beijing, China, 2017.
4. Pashin, J.C. Stratigraphy and structure of coalbed methane reservoirs in the United States: An overview. *Int. J. Coal Geol.* **1998**, *35*, 209–240. [CrossRef]
5. Pashin, J.C. Geology of North American coalbed methane reservoirs. In *Coal Bed Methane: Theories and Applications*; Elsevier: Amsterdam, The Netherlands, 2020.
6. Groshong, R.H.; Pashin, J.C.; Mcintyre, M.R. Structural controls on fractured coal reservoirs in the southern Appalachian Black Warrior foreland basin. *J. Struct. Geol.* **2009**, *31*, 874–886. [CrossRef]
7. Jiang, B.; Qu, Z.H.; Wang, G.; Li, M. Effects of structural deformation on formation of coalbed methane reservoirs in Huaibei coalfield, China. *Int. J. Coal Geol.* **2010**, *82*, 175–183. [CrossRef]
8. Jing, B.; Li, M.; Song, Y.; Cheng, G.X.; Zhu, G.Y. *Tectonically Deformed Coal and Its Gas Geological Significance*; Science Press: Beijing, China, 2020.
9. Li, M.; Jiang, B.; Lin, S.F.; Lan, F.J.; Wang, J.L. Structural controls on coalbed methane reservoirs in Faer coal mine, Southwest China. *J. Earth Sci.* **2013**, *24*, 437–448. [CrossRef]
10. Chen, Y.; Tang, D.Z.; Xu, H.; Li, Y.; Meng, Y.J. Structural controls on coalbed methane accumulation and high production models in the eastern margin of Ordos Basin, China. *J. Nat. Gas Sci. Eng.* **2015**, *23*, 524–537. [CrossRef]
11. Zhu, H.Z.; Liu, P.; Chen, P.; Kang, J.N. Analysis of coalbed methane occurrence in Shuicheng Coalfield, southwestern China. *J. Nat. Gas Sci. Eng.* **2017**, *47*, 140–153. [CrossRef]
12. Guo, X.J.; Huan, X.; Huan, H.H. Structural characteristics of deformed coals with different deformation degrees and their effects on gas adsorption. *Energy Fuels* **2017**, *31*, 13374–13381. [CrossRef]
13. Liu, H.W.; Jiang, B. Geochemical alteration and mineralogy of coals under the influence of fault motion: A case study of Qi'nan colliery, China. *Minerals* **2019**, *9*, 389. [CrossRef]

14. Lu, Y.J.; Liu, D.M.; Cai, Y.D.; Li, Q.; Jia, Q.F. Pore-fractures of coalbed methane reservoir restricted by coal facies in Sangjiang-Muling coal-bearing Basins, Northeast China. *Minerals* **2020**, *13*, 1196. [CrossRef]
15. Hower, J.C.; Davis, A. Vitrinite reflectance anisotropy as a tectonic fabric element. *Geology* **1981**, *9*, 165–168. [CrossRef]
16. Li, Z.; Liang, Z.K.; Jiang, Z.X.; Yu, H.L.; Yang, Y.D.; Xiao, L. Pore connectivity characterization of lacustrine shales in Changling fault depression, Songliao Basin, China: Insights into the effects of mineral compositions on connected pores. *Minerals* **2019**, *9*, 198. [CrossRef]
17. Liu, X.F.; He, X.Q. Effect of pore characteristics on coalbed methane adsorption in middle-high rank coals. *Adsorption* **2017**, *23*, 3–12. [CrossRef]
18. Mastalerz, M.; He, L.; Melnichenko, Y.B.; Rupp, J.A. Porosity of coal and shale: Insights from gas adsorption and SANS/USANS techniques. *Energy Fuels* **2012**, *26*, 5109–5120. [CrossRef]
19. Yao, H.F.; Kang, Z.Q.; Li, W. Deformation and reservoir properties of tectonically deformed coals. *Petrol. Explor. Dev.* **2014**, *41*, 460–467. [CrossRef]
20. Karayiğit, A.İ.; Mastalerz, M.; Oskay, R.G.; Buzkan, İ. Bituminous coal seams from underground mines in the Zonguldak Basin (NW Turkey): Insights from mineralogy, coal petrography, Rock-Eval pyrolysis, and meso-and microporosity. *Int. J. Coal Geol.* **2018**, *199*, 91–112. [CrossRef]
21. Wei, C.T.; Qin, Y.; Wang, G.X.; Fu, X.H.; Zhang, Z.Q. Numerical simulation of coalbed methane generation, dissipation and retention in SE edge of Ordos Basin, China. *Int. J. Coal Geol.* **2010**, *82*, 147–159. [CrossRef]
22. Casey, M.; Butler, R.W.H. Modelling approaches to understanding fold development: Implications for hydrocarbon reservoirs. *Mar. Petrol. Geol.* **2004**, *21*, 933–946. [CrossRef]
23. Shen, J.; Fu, X.H.; Qin, Y.; Liu, Z. Control actions of structural curvature of coal-seam floor on coalbed gas in the No. 8 coal mine of Pingdingshan. *J. China Coal Soc.* **2010**, *35*, 586–589.
24. Fu, H.J.; Tang, D.Z.; Xu, T.; Xu, H.; Tao, S.; Zhao, J.L.; Chen, B.L.; Yin, Z.Y. Preliminary research on CBM enrichment models of low-rank coal and its geological controls: A case study in the middle of the southern Junggar Basin, NW China. *Mar. Petrol. Geol.* **2017**, *83*, 97–110. [CrossRef]
25. Pashin, J. Variable gas saturation in coalbed methane reservoirs of the Black Warrior Basin: Implications for exploration and production. *Int. J. Coal Geol.* **2010**, *82*, 135–146. [CrossRef]
26. Zhang, Z.G.; Qin, Y.; Yi, T.S.; You, Z.J.; Yang, Z.B. Pore structure characteristics of coal and their geological controlling factors in the eastern Yunnan and western Guizhou, China. *ACS Omega* **2020**, *5*, 19565–19578. [CrossRef]
27. Zhang, Z.M.; Wu, Y. *China Coalmine Gas-Geologic Laws and Mapping*; China University of Mining and Technology Press: Xuzhou, China, 2014.
28. Li, S.; Tang, D.Z.; Pan, Z.J.; Xu, H.; Guo, L.L. Evaluation of coalbed methane potential of different reservoirs in western Guizhou and eastern Yunnan, China. *Fuel* **2015**, *139*, 257–267. [CrossRef]
29. Lan, F.J.; Qin, Y.; Wang, A.K.; Li, M.; Wang, G.X. The origin of high and variable concentrations of heavy hydrocarbon gases in coal from the Enhong syncline of Yunnan, China. *J. Nat. Gas Sci. Eng.* **2020**, *76*, 1–11. [CrossRef]
30. Cheng, G.X.; Jiang, B.; Li, M.; Li, F.L.; Xu, S.C. Quantitative characterization of fracture structure in coal based on image processing and multifractal theory. *Int. J. Coal Geol.* **2020**, *228*, 1–20.
31. Zhang, G.W.; Guo, A.L.; Wang, Y.J.; Li, S.Z.; Dong, Y.P.; Liu, S.F.; He, D.F.; Cheng, S.Y.; Lu, R.K.; Yao, A.P. Tectonics of South China continent and its implications. *Sci. China-Earth Sci.* **2013**, *56*, 1804–1828. [CrossRef]
32. Qiu, L.; Yan, D.P.; Yang, W.X.; Wang, J.B.; Tang, X.L.; Ariser, S. Early to Middle Triassic sedimentary records in the Youjiang Basin, South China: Implications for Indosinian orogenesis. *J. Asian Earth Sci.* **2017**, *141*, 125–139. [CrossRef]
33. Lan, F.J.; Qin, Y.; Li, M.; Lin, Y.C.; Wang, A.K.; Shen, J. Abnormal concentration and origin of heavy hydrocarbon in upper Permian coal seams from Enhong syncline, Yunnan, China. *J. Earth Sci.* **2012**, *23*, 842–853. [CrossRef]
34. Li, M.; Jiang, B.; Liu, J.G.; Zhu, P.; Cheng, G.X. Geological models and structural controls of tectonically deformed coal in Tucheng syncline, western Guizhou Province. *J. China Coal Soc.* **2018**, *42*, 726–731.
35. Wan, T.F. *The Tectonics of China: Data, Maps and Evolution*; Higher Education Press: Beijing, China, 2011.
36. Hou, Y.G.; He, S.; Tang, D.Q. Tectonic reverse of Cenozoic basins and its relationship with the biogas accumulation in north-east of Yunnan Province. *J. Cent. South Univ.* **2012**, *43*, 2238–2246.

37. Spiro, B.F.; Liu, J.J.; Dai, S.F.; Zeng, R.S.; Large, D.; French, D. Marine derived $^{87}Sr/^{86}Sr$ in coal, a new key to geochronology and palaeoenvironment: Elucidation of the India-Eurasia and China-Indochina collisions in Yunnan, China. *Int. J. Coal Geol.* **2019**, *215*, 103304. [CrossRef]
38. Liu, H.P.; Wang, Z.C.; Xiong, B.X.; Li, Y.L.; Liu, L.Q.; Zhang, J.Z. Coupling analysis of Mesozoic-Cenozoic foreland basin and mountain system in central and western China. *Geosci. Front.* **2000**, *7*, 55–72.
39. Lan, F.J.; Qin, Y.; Li, M.; Tang, Y.H.; Guo, C.; Zhang, F. Microbial degradation and its influence on components of coalbed gases in Enhong syncline, China. *Int. J. Min. Sci. Technol.* **2013**, *23*, 293–299. [CrossRef]
40. Li, M.; Jiang, B.; Lin, S.F.; Lan, F.J.; Zhang, G.S. Characteristics of coalbed methane reservoirs in Faer Coalfield, Western Guizhou. *Energy Explor. Exploit.* **2013**, *31*, 411–428. [CrossRef]
41. Qin, Y.; Xiong, M.H.; Yi, T.S.; Yang, Z.B.; Wu, C.F. On unattached multiple superposed coalbed-methane system: In a case of the Shuigonghe syncline, Zhijin-Nayong coalfield, Guizhou. *Geol. Rev.* **2008**, *54*, 65–70.
42. Shen, Y.L.; Qin, Y.; Guo, Y.H.; Yi, T.S.; Yuan, X.X.; Shao, Y.B. Characteristics and sedimentary control of a coalbed methane-bearing system in Lopingian (late Permian) coal bearing strata of western Guizhou Province. *J. Nat. Gas Sci. Eng.* **2016**, *33*, 8–17. [CrossRef]
43. Wang, Y.Z.; Cao, Y.C.; Wang, S.P.; Song, Y.B. Advances in research of spatial structures of unconformity. *Geotecton. Metallog.* **2006**, *30*, 326–330.
44. Zhang, R.X.; Wang, X.Z.; Lan, D.Q.; Kang, B.P. Reservoir evaluation of Emeishan basalts in Southwest Sichuan. *Nat. Gas Explor. Dev.* **2006**, *29*, 17–20.
45. Tang, S.L.; Tang, D.Z.; Xu, H.; Tao, S.; Li, S.; Geng, Y.G. Geological mechanisms of the accumulation of coalbed methane induced by hydrothermal fluids in the western Guizhou and eastern Yunnan regions. *J. Nat. Gas Sci. Eng.* **2016**, *33*, 644–656. [CrossRef]
46. Tao, S.; Tang, D.Z.; Qin, Y.; Xu, H.; Li, S.; Cai, J.L. Analysis on thermal history of coal strata of typical mining areas in western Guizhou and eastern Yunnan. *Coal Geol. Explor.* **2010**, *38*, 17–21.
47. Dou, X.Z.; Jiang, B.; Qin, Y.; Qu, Z.H.; Yang, Z.B.; Wu, Y.Y. Pattern and mechanism of metamorphism of late Permian coal in western Guizhou. *J. China Coal Soc.* **2012**, *37*, 424–429.
48. Song, Y.; Zhao, M.J.; Liu, S.B.; Wang, H.Y.; Chen, Z.H. The influence of tectonic evolution on the accumulation and enrichment of coalbed methane (CBM). *Chin. Sci. Bull.* **2005**, *50*, 1–6. [CrossRef]